Can robots patch-clamp as well as humans? Characterization of a novel sodium channel mutation

M. Estacion[1,2,3], J. S. Choi[1,2,3], E. M. Eastman[1,2,3], Z. Lin[4], Y. Li[4], L. Tyrrell[1,2,3], Y. Yang[4], S. D. Dib-Hajj[1,2,3] and S. G. Waxman[1,2,3]

[1]*Department of Neurology and* [2]*Center for Neuroscience and Regeneration Research, Yale University School of Medicine, New Haven, CT 06510, USA*
[3]*Rehabilitation Research Center, Veterans Affairs Connecticut Healthcare System, West Haven, CT 06516, USA*
[4]*Department of Dermatology, Peking University First Hospital, Beijing, 100034, China*

Ion channel missense mutations cause disorders of excitability by changing channel biophysical properties. As an increasing number of new naturally occurring mutations have been identified, and the number of other mutations produced by molecular approaches such as *in situ* mutagenesis has increased, the need for functional analysis by patch-clamp has become rate limiting. Here we compare a patch-clamp robot using planar-chip technology with human patch-clamp in a functional assessment of a previously undescribed $Na_v1.7$ sodium channel mutation, S211P, which causes erythromelalgia. This robotic patch-clamp device can increase throughput (the number of cells analysed per day) by 3- to 10-fold. Both modes of analysis show that the mutation hyperpolarizes activation voltage dependence (−8 mV by manual profiling, −11 mV by robotic profiling), alters steady-state fast inactivation so that it requires an additional Boltzmann function for a second fraction of total current (∼20% manual, ∼40% robotic), and enhances slow inactivation (hyperpolarizing shift −15 mV by human, −13 mV robotic). Manual patch-clamping demonstrated slower deactivation and enhanced (∼2-fold) ramp response for the mutant channel while robotic recording did not, possibly due to increased temperature and reduced signal-to-noise ratio on the robotic platform. If robotic profiling is used to screen ion channel mutations, we recommend that each measurement or protocol be validated by initial comparison to manual recording. With this caveat, we suggest that, if results are interpreted cautiously, robotic patch-clamp can be used with supervision and subsequent confirmation from human physiologists to facilitate the initial profiling of a variety of electrophysiological parameters of ion channel mutations.

(Received 15 December 2009; accepted after revision 25 January 2010; first published online 1 February 2010)
Corresponding author S. G. Waxman: Neuroscience Research Center, Bldg 34, VA Connecticut Healthcare System (127A), 950 Campbell Avenue, West Haven, CT 06516, USA. Email: stephen.waxman@yale.edu

Abbreviations DRG, dorsal root ganglion; hERG, human *ether-à-go-go* related gene; IEM, inherited erythromelalgia; S211P, serine 211 to proline mutant.

Introduction

The discovery of hundreds of new ion channel mutations linked to disorders of excitation (George, 2005; Claes *et al.* 2009; Lossin, 2009) presents physiologists with the challenge of functionally assessing their pathophysiological impact because many of these mutations cause disease by changing the channel's biophysical properties. Molecular methods such as *in situ* mutagenesis for investigating structure–function relationships or the role of specific residues in post-translational channel modifications have further increased the need for functional analysis. Selective amino-acid substitutions, for example, have demonstrated roles for large hydrophobic residues in channel gating (Lampert *et al.* 2008), and alanine-scanning (McPhee *et al.* 1998) and cysteine-scanning mutagenesis (Sheets & Hanck, 2007) create multiple channel variants that require electrophysiological characterization.

Biophysical characterization of heterologously expressed ion channels via patch-clamp requires formation of a gigaohm seal between the recording electrode and cell membrane. Recently, higher-throughput electrophysiology platforms, using planar patch-clamp (Ghetti *et al.* 2007; Dunlop *et al.* 2008) to obtain gigaohm seals have been used to screen compound libraries for channel modulators and lead compound optimization (Trivedi *et al.* 2008; Castle *et al.* 2009), and

DOI: 10.1113/jphysiol.2009.186114

to screen for off-target (e.g. cardiac) side-effects against channels such as hERG (Tao *et al.* 2004; Dubin *et al.* 2005; Brown, 2009). These automated platforms have been validated against manual patch-clamp with respect to compound potencies (Bruggemann *et al.* 2003; Kiss *et al.* 2003) but not with respect to measurement of voltage dependence or kinetics.

Here we compare functional assessment of a newly identified sodium channel mutation by a robotic planar patch-clamp platform with assessment by experienced human patch-clampers. The $Na_V1.7$ voltage-gated sodium channel is preferentially expressed within dorsal root ganglion (DRG) neurons (Felts *et al.* 1997; Sangameswaran *et al.* 1997; Toledo-Aral *et al.* 1997), especially nociceptors (Djouhri *et al.* 2003), where it sets the gain on pain signalling (Waxman, 2006). Mutations of $Na_V1.7$ have been shown to cause inherited erythromelalgia (IEM), a disorder characterized by severe pain in the limbs. These mutations hyperpolarize $Na_V1.7$ activation, slow deactivation, and enhance ramp currents (Dib-Hajj *et al.* 2007). Here we evaluate the capability of a robotic patch-clamp system to assess these and other parameters.

Methods

Exon screening

This study conformed with the *Declaration of Helsinki*. A 15-year-old Chinese male, without a family history of a pain disorder, was diagnosed with erythromelalgia. Family consent was obtained according to an approved institutional review board protocol, and blood samples were withdrawn and analysed for mutations in *SCN9A* (sodium channel gene 9A) which encodes the $Na_V1.7$ channel. Genomic DNA was screened for mutations in *SCN9A* as described previously (Yang *et al.* 2004); comparison to reference $Na_V1.7$ cDNA (Klugbauer *et al.* 1995) identified sequence variation.

Plasmid and stable cell line

For cell transfection, human $Na_V1.7$ (Klugbauer *et al.* 1995) was converted to tetrodotoxin resistant ($hNa_V1.7_R$) by Y362S substitution (Herzog *et al.* 2003), which will be referred to as wild-type (WT) hereafter. The S211P mutation was introduced using QuickChange XLII site-directed mutagenesis (Stratagene, La Jolla, CA, USA). Transfected HEK 293 cells in Dulbeccos's modified Eagle's medium supplemented with 10% fetal bovine serum were treated with genenticin (G418) for several weeks to derive stable cell lines that express the WT and S211P mutant sodium channels. A clonal cell line for each channel that expressed robust Na^+ current in the majority of cells was selected for biophysical characterization.

Manual electrophysiology

The extracellular solution for whole-cell voltage-clamp recordings contained (in mM): 140 NaCl, 3 KCl, 1 $MgCl_2$, 1 $CaCl_2$, 10 Hepes, pH 7.3 with NaOH (adjusted to 320 mosmol l^{-1} with dextrose). The pipette solution contained (in mM): 140 CsF, 10 NaCl, 2 $MgCl_2$, 1 EGTA, 10 Hepes, pH 7.3 with CsOH (adjusted to 310 mosmol l^{-1} with dextrose). Patch-pipettes had a resistance of 1–3 MΩ when filled with pipette solution. The junction potential of 9 mV (calculated by JPcalc included in pCLAMP software) was compensated by setting the holding potential during the seal test period to −9 mV. Once the seal had formed, these two solutions were no longer in contact and the applied potential was correct. Upon achieving whole-cell configuration, the cells were maintained at a holding potential of −100 mV. Pipette and cell capacitance were manually minimized using Axopatch 200B (Molecular Devices, Union City, CA, USA) compensation circuitry. To reduce voltage errors, 80–90% series resistance and prediction compensation were applied. Cells with >3 mV voltage error were excluded from analysis. Recorded currents were digitized using pCLAMP (v.10) and a Digidata 1440A interface (Molecular Devices) at a rate of 50 kHz after passing through a low-pass Besssel filter with a setting of 10 kHz. Na^+ current recordings began 5 min after achieving the whole-cell configuration.

Data analysis was performed using Clampfit (Molecular Devices) or Origin (OriginLab Corp., Northampton, MA, USA) software. Peak inward currents from activation protocols were converted to conductances using the equation $G = I/(V_m - E_{Na})$, where G is the conductance, I is the peak inward current, V_m is the membrane potential step used to elicit the response and E_{Na} is the reversal potential for sodium (determined for each cell using the x-axis intercept of a linear fit of the peak inward current responses). Conductances were normalized to maximum conductance and fitted with a Boltzmann equation of the form:

$$G = G_{min} + (G_{max} - G_{min})/(1 + \exp[(V_{1/2} - V_m)/k)],$$

where $V_{1/2}$ is half-activation potential, G_{max} and G_{min} are maximum and minimum conductance, and k is a slope factor. Peak inward currents from steady-state fast inactivation and slow inactivation protocols were normalized to maximum current and fitted with a Boltzmann equation of the form:

$$I = I_{min} + (I_{max} - I_{min})/(1 + \exp[(V_m - V_{1/2})/k)],$$

where V_m represents inactivating pre-pulse membrane potential. Decaying currents were fitted with a single exponential equation:

$$I = A \exp(-t/\tau) + I_c,$$

where A is fit amplitude, t is time, τ is the decay time constant and I_c is the asymptotic current decay minimum. Data are expressed as means ± standard error of the mean (S.E.M.). Statistical significance was determined by Student's t test.

Planar patch-clamp electrophysiology (robotic)

We assessed the PatchXpress robotic electrophysiology platform from Molecular Devices. This incorporates eight MultiClamp 700A dual amplifiers to provide 16 independent simultaneous recordings, digitized by a Digidata1440A. Recordings were obtained using a planar patch-clamp array of 16 wells of 1–2 μm aperture (Sealchip16; Aviva Biosciences, San Diego, CA, USA). Extracellular and intracellular solutions were the same as for manual patch-clamp recordings. Cells were harvested by washing a 100 mm dish of 70–90% confluent stably transfected HEK 293 cells two times with divalent-free PBS, followed by 0.05% trypsin/EDTA, with subsequent detachment of cells with gentle tituration using complete medium to inactivate the trypsin. Cells were pelleted by centrifugation (900 g, 1.5 min) and the pellet resuspended (1×10^6 cells ml^{-1}) in incomplete DMEM and allowed to recover for 20 min at 37°C. To minimize possible variations over time in culture, cells stably expressing WT or S211P channels were recorded on the same day.

Computer-controlled capture, gigaohm sealing, and rupture using PatchXpress protocols achieved the whole-cell recording configuration. The liquid junction potential of 9 mV was compensated by specifying the value in the PatchXpress software. To reduce voltage errors, the degree of series resistance and prediction compensation were specified (in advance) in the experimental procedure file at 50% except for the preliminary dataset shown in Fig. 2 when the compensation was set to 80%. This preliminary dataset shown in Fig. 2 was also performed with a holding potential of −120 mV and with no junction potential correction. All the results reported directly comparing the robotic patch-clamp to manual patch-clamp were performed at the matched holding potential of −100 mV and junction potential correction applied. The order, timing and specification of all stimulation protocols were identical to those for manual recording. The signals from 16 cells were multiplexed and then digitized by a single Digidata1440A at a maximal rate of 31.25 kHz after passing through a low-pass Besssel filter setting of 10 kHz under the control of PatchXpress software, which builds upon pCLAMP's Clampex software capabilities. Data were stored and analysed using DataXpress (Molecular Devices) with a structured query language (SQL) database coupled to an enhanced Clampfit allowing automated analysis of recorded data, which can be extracted by criteria and grouped into datasets (e.g. activation trials on a particular channel grouped into a dataset for analysis). Similar to manual analysis using Clampfit, cursor pairs were specified so that measurements (e.g. peak amplitude, time-to-peak and exponential fits to determine kinetics) could be extracted. For analysis of kinetics, however, the positions of the cursors were saved globally for the trial as mandated by the software, whereas for manual analysis the positions of the cursors was adjustable for each sweep of the trial. Although the data sweeps can be exported for analysis in other programs, the analysis of kinetic data in the automated patch-clamp figures are shown as analysed by DataXpress with fixed cursor positions.

Results

S211P mutation

Sequence analysis of *SCN9A* coding exons demonstrated T-to-C substitution (c.631T>C) in exon 5 in the proband, replacing serine 211 with proline (S211P) near the extracellular N-terminus end of the domain I S4 segment (DI/S4), altering a highly conserved amino acid. The c.631T>C mutation was absent from 200 normal Chinese control alleles, indicating that it is unlikely to be a benign polymorphism.

Parsing of robotic data for analysis

Cells were randomly sealed to the robotic patch-clamp planar chip. A schematic diagram illustrating a planar glass substrate chip is shown in Fig. 1*A*. Using the robotic apparatus, an aliquot of harvested cells in suspension is added to the well of the chip and a recording is obtained from the first cell to land on the hole without further selection. Manual patch-clamp with a glass micropipette (Fig. 1*B*), in contrast, allows for visual selection using criteria such as cell appearance, size and expression of visual markers such as green fluorescent protein. Inherent to the robotic system's recording in this non-selective manner, we found that some cells needed to be excluded from the analysis. Notable examples of excluded cells are shown in Fig. 1. Interpretable G–V curves that were well fitted by the Boltzmann equation required a well-formed I–V relationship. For these curves, a linear fit between +10 mV and +30 mV determined the reversal potential (E_{Na}) for transformation of the I–V curve into a G–V curve (Fig. 1*C*); cells with G–V curves that did not match this criterion were excluded. In addition to recording from cells that a human physiologist would accept for analysis, the robotic device recorded from several groups of cells that experienced human patch-clampers would exclude. Additional exclusion criteria included (i) cells showing oscillations or ringing due to poorly adjusted series

resistance compensation that did not yield well-formed *I–V* curves (Fig. 1*D*); (ii) cells showing contamination by slowly gated outward currents (Fig. 1*E*); (iii) cells with small peak inward current (<350 pA); and (iv) cells having large (>15 mV) uncompensated series resistance error. Each of these groups of cells yielded poorly formed *I–V* curves and, if encountered by human patch-clampers, would have been eliminated from further analysis.

A preliminary data display, in which PatchXpress produced a dataset from all recorded WT cells ($n = 64$) with activation protocol data recorded using series resistance compensation of 80% is shown in Fig. 2*A*, with each cell plotted as a coloured line and averages of all data at each potential plotted as filled circles. When the analysis was performed on each cell to fit a Boltzmann relation, the mean $V_{1/2}$ was -9.3 ± 14 mV with a slope factor k of 7.3 ± 2.2.

We next filtered this unselected cell population by sequentially eliminating each of the groups of cells that would have been eliminated by experienced human patch-clampers. Manual elimination of oscillating cells in this dataset removed 17 of 64 recorded cells (Fig. 2*B*). Since most oscillating cells showed current at all potentials, the average was improved by reducing the offset at subthreshold potentials. After elimination of oscillating cells, the mean $V_{1/2}$ was -24.5 ± 3.1 mV and $k = 6.3 \pm 0.7$ ($n = 47$). Subsequent removal of an additional 17 cells with peak currents <350 pA (Fig. 2*C*) yielded a mean $V_{1/2}$ of -24.4 ± 4.3 mV, $k = 5.0 \pm 0.6$ ($n = 30$). Finally (Fig. 2*D*), removing cells contaminated by other currents (9 of 64 cells), and with uncompensated series resistance error ≥15 mV (6 of 64 cells) gave a mean $V_{1/2}$ of -27.1 ± 1.7 mV, $k = 6.0 \pm 0.4$ ($n = 15$).

As a measure of whether there are criteria that might be automatically substituted for operator-selected cell elimination by visual criteria, cells were alternatively selected based on the linear fit for E_{Na} (Fig. 2*E*).

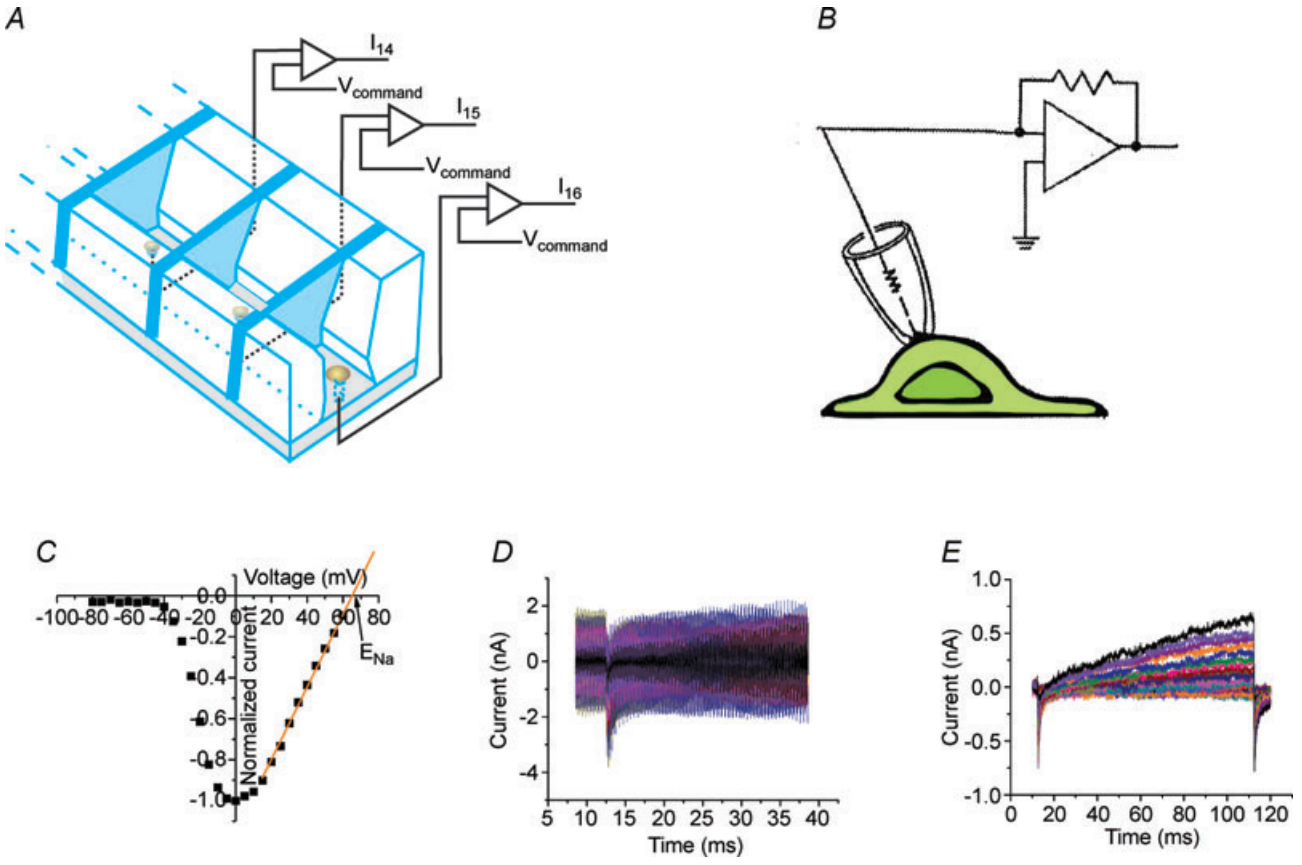

Figure 1. Robotic patch-clamp records from cells randomly
A, schematic drawing of a planar patch-clamp chip recording configuration. *B*, schematic drawing of a conventional patch-clamp recording configuration. *C*, example of a well-formed voltage-gated sodium channel *I–V* curve. The first step to fitting *I–V* data with a Boltzmann equation is to transform the *I–V* curve into a *G–V* curve. Values of E_{Na} are determined on a cell-by-cell basis by fitting a straight line to the linear portion of the *I–V* curve (usually between +10 mV and +40 mV). *D*, some cells were not appropriate for analysis because of oscillations due to incomplete series resistance compensation tuning. Data sweeps show oscillatory behaviour for the illustrated cell. *E*, example of other cells excluded because they were contaminated by uncharacterized currents that distort the *I–V* relation; a left-shifted reversal potential for this cell.

The criterion that $+40\,mV \leq E_{Na} \leq +90\,mV$ (mean $E_{Na} + 65\,mV$) eliminated most of the oscillating and outward current-contaminated cells. Although use of this criterion did not remove all of the small-peak-current cells, it yielded a mean $V_{1/2}$ of -26.6 ± 1.7 mV, $k = 6.3 \pm 0.6$ ($n = 28$), close to the value achieved by manual elimination of problematic cells as described above.

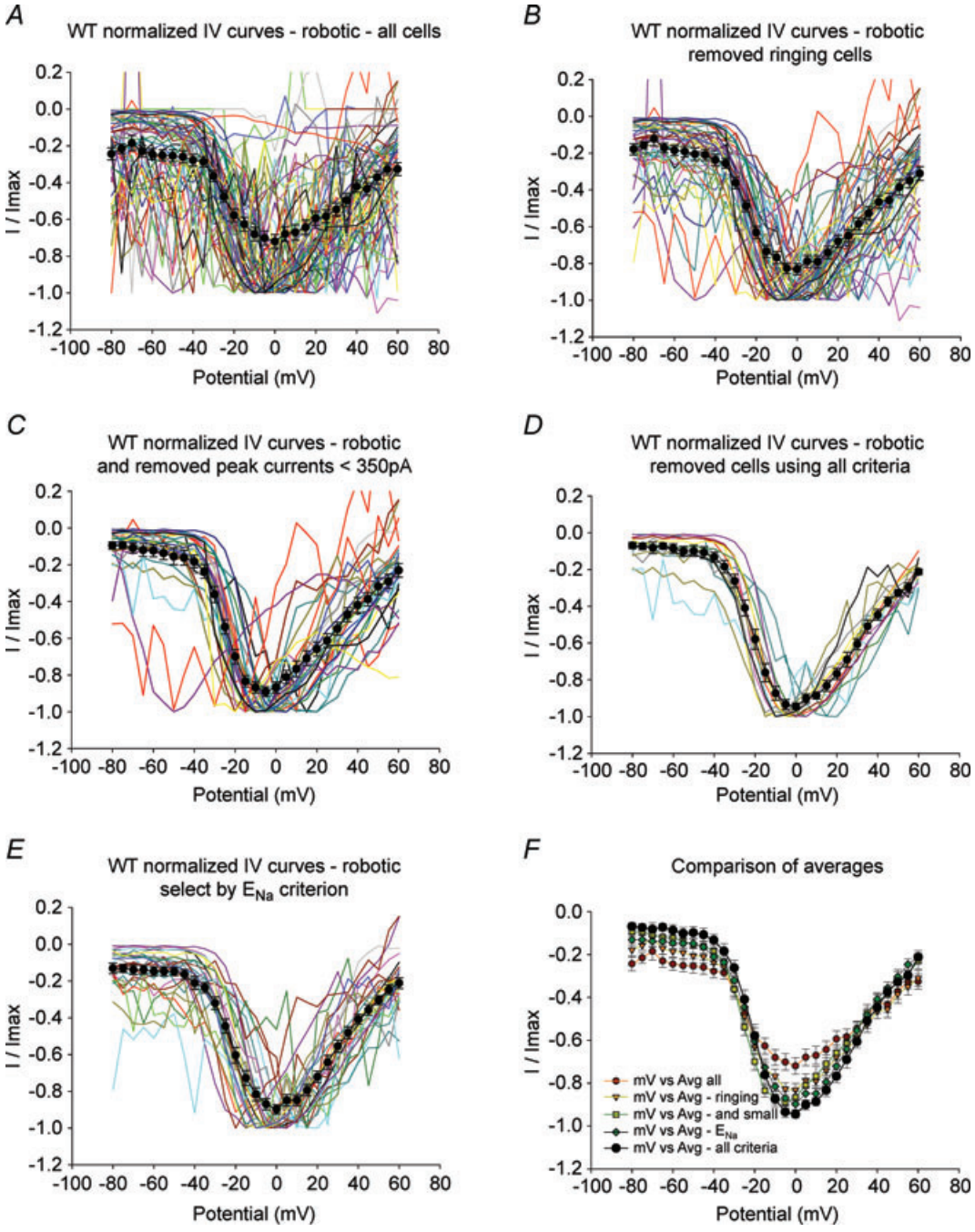

Figure 2. Parsing of robotic patch-clamp data
A, normalized *I–V* relations of a preliminary dataset of $Na_V1.7$-WT cells recorded by robotic patch-clamp are displayed as coloured lines. *B*, the first selection criterion removed oscillating cells (in this dataset, 17 out of 64 cells). *C*, the next selection criterion removed cells with peak currents <350 pA (17 out of 64 cells). *D*, a final set of cells for analysis was obtained by removing cells contaminated by other currents (9 out of 64 cells) and cells whose uncompensated series resistance error exceeded 15 mV (6 out of 64 cells). *E*, based on the linear fit for E_{Na}, the criterion that $+40\,mV < E_{Na} < +90\,mV$ (average E_{Na}, +65 mV) removed most of the oscillating and outward-current-contaminated cells but did not remove all of the cells producing <350 pA currents. *F*, comparison of the average *I–V* curves as criteria are applied.

Voltage-clamp recordings

To compare manual and robotic patch-clamp, whole-cell voltage-clamp recordings were performed on clonal cell lines stably expressing WT or S211P channels. Voltage-clamp recordings on the robotic platform were matched to the manual recording protocols with the exception that series resistance compensation was reduced to 50% to minimize the number of oscillating cells. Activation properties were measured by applying 100 ms test pulses to potentials between −80 and +40 mV in 5 mV increments. Manual (Fig. 3*A* and *B*, representative traces) and robotic (Fig. 3*C* and *D*, representative traces) recordings displayed similar inward currents, but the average peak inward current for S211P cells was significantly smaller compared to WT cells (Table 1).

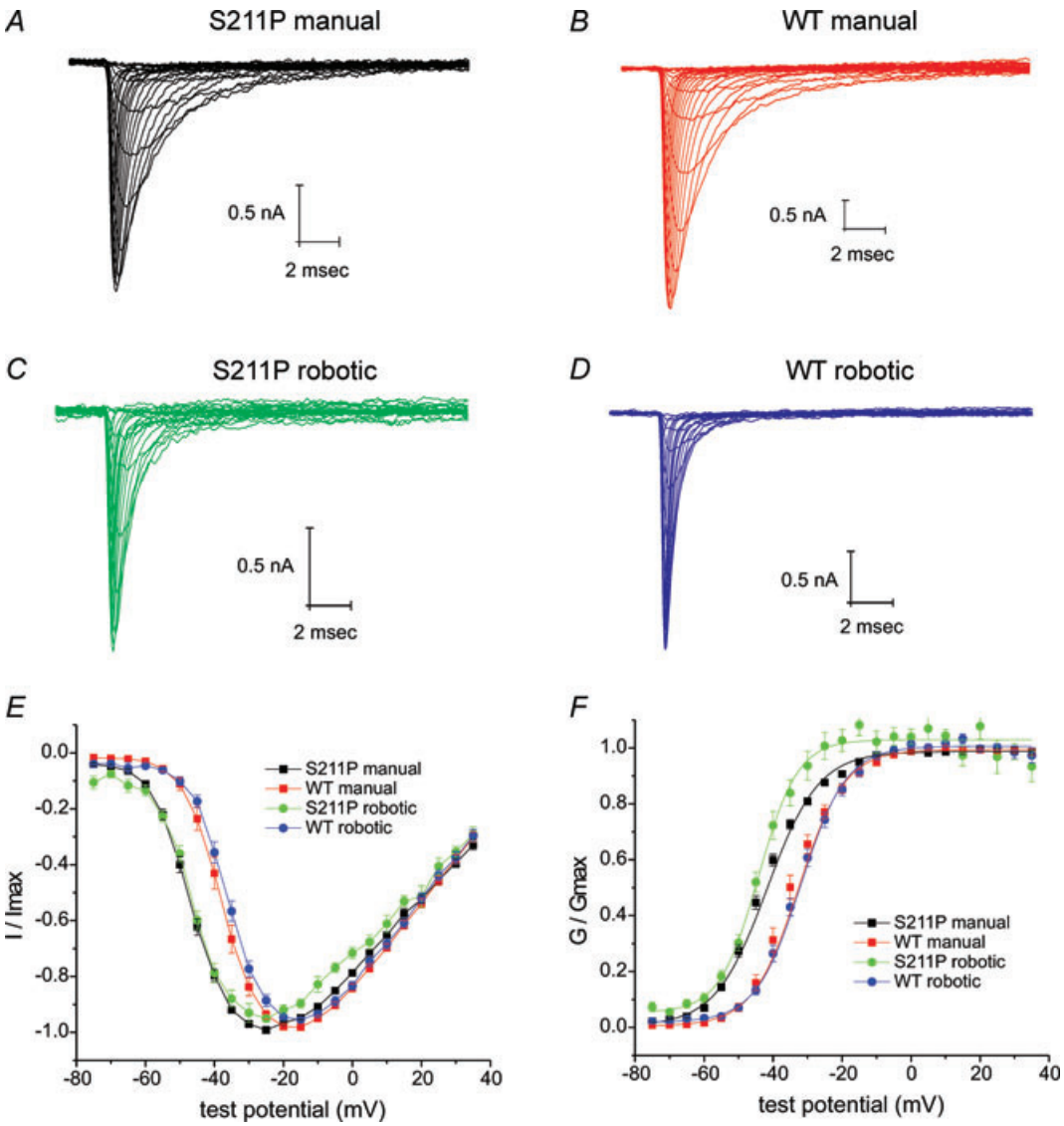

Figure 3. Activation properties
A–D, typical data traces recorded from HEK 293 cell lines expressing the WT or S211P mutant channels. Current densities from the S211P-expressing cell line were lower than in the WT cell line (note relative sizes of vertical scale bars). For display purposes the traces were digitally filtered to 2 kHz. *E*, peak current–voltage data are normalized to I_{MAX} for each cell, then averaged, and plotted as a function of test potential. Manual data for S211P are shown using black squares ($n = 24$) and manual data for WT using red squares ($n = 18$). Robotic S211P data are shown using green circles ($n = 16$) and robotic WT data using blue circles ($n = 59$). Error bars are ± S.E.M. *F*, the conductance–voltage curves derived from the *I–V* data as described in the Methods and normalized to the value of G_{max} derived from the Boltzmann fit are averaged and plotted as a function of test potential. Error bars are ± S.E.M.

Table 1. Comparison of manual *vs.* robotic patch-clamp

Parameter	Manual			Robotic		
Cell preparation	Attached to coverslip			Cell suspension		
Cell selection	Visual			Random		
Ambient temp	20–22°C			24–27°C		
	S211P		WT	S211P		WT
General						
Total cells	24		24	126		101
Cells meeting selection criterion	24 (100%)		18 (75%)	16 (13%)		59 (58%)
Mean peak Na^+ current (nA)	−2.1 ± 0.2		−4.8 ± 0.5	−0.79 ± 0.16		−1.9 ± 0.2
Mean cell capacitance (pF)	19.7		17.7	8.9 ± 0.7		11.5 ± 0.9
Mean current density (pA pF^{-1})	−111 ± 13		−270 ± 24	−43 ± 28		−170 ± 16
Mean access resistance (MΩ)	3.3		3.2	6.0 ± 0.3		5.8
R_s comp range (%)	80–95		80–95	50		50
Mean uncompensated V_m error (mV)	−0.96		−1.8	−2.9 ± 0.6		−6.8
Activation						
Mean activation $V_{1/2}$ (mV)	−42.9 ±0.9		−34.7 ± 1.2	−42.8 ± 1.4		−31.8 ± 0.9
Change from WT (mV)	−8.2	$P < 0.001$		−11	$P < 0.001$	
Mean activation slope	7.6 ± 0.3		6.4 ± 0.2	6.4 ± 1		6.4 ± 0.3
Change from WT	1.2	$P < 0.01$		0	n.s.	
Time to peak at −50 mV (ms)	1.44 ± 0.09		1.96 ± 0.19	1.04 ± 0.08		2.02 ± 0.32
Change from WT (ms)	−0.52	$P < 0.01$		−0.98	$P < 0.05$	
Inactivation rate at −45 mV (ms)	3.26 ± 0.41		5.17 ± 0.64	1.48 ± 0.12		2.57 ± 0.31
Change from WT (ms)	−1.91	$P < 0.05$		−1.09	$P < 0.05$	
Deactivation rate at −60 mV (ms)	0.23 ± 0.02		0.16 ± 0.02	0.11 ± 0.01		0.11 ± 0.01
Change from WT (ms)	0.07	$P < 0.05$		0	n.s.	
Fast inactivation						
Mean fast inactivation $V_{1/2}$ major (mV)	−87.4 ± 0.9		−87.4 ± 1.6	−88.4 ± 2.9		−86.1 ± 1.3
Change from WT (mV)	0	n.s.		−2.	n.s.	
Mean fast inactivation slope major	4.8 ± 0.3		5.3 ± 0.5	6.1 ± 2.3		5.3 ± 0.5
Change from WT	0.5	n.s.		0.8	n.s.	
Mean fast inactivation $V_{1/2}$ minor (mV)	−116.3 ±2.4		−109.4 ±3.2	−117.3 ± 3.4		−107.6 ± 3.4
Change from WT (mV)	−6.9	$P = 0.08$		−9.7	$P = 0.08$	
Mean fast inactivation slope minor	12.7 ± 0.6		9.9 ± 1.0	18.4 ± 2.8		13.7 ± 2.4
Change from WT	2.8	$P < 0.05$		4.7	n.s.	
Fraction (minor/total) (%)	27 ± 2		25 ± 5	54 ± 5.2		43 ± 4.1
Repriming at −100 mV (ms)	45.3 ± 4.0		50.5 ± 10.5	20.2 ± 8.0		27.6 ± 6.2
Change from WT (ms)	−5.2	n.s.		−7.4	n.s.	
Slow inactivation						
Mean slow inactivation $V_{1/2}$ (mV)	−92.9 ± 2.3		−77.8 ± 3.7	−94.1 ± 1.3		−79.7 ± 1.7
Change from WT (mV)	−15.1	$P < 0.001$		−14.4	$P < 0.001$	
Mean slow inactivation slope	7.5 ± 0.6		14.1 ± 1.3	6.3 ± 0.4		8.4 ± 0.4
Change from WT	6.6	$P < 0.001$		2.1	$P < 0.05$	
Ramps						
Mean slow ramp peak amplitude (%)	1.59 ± 0.15		0.78 ± 0.12	1.47 ± 0.47		1.04 ± 0.26
Change from WT	2-fold	$P < 0.05$		1.5-fold	n.s.	
Mean slow ramp voltage at peak (mV)	−62.6 ± 1.1		−52.2 ± 1.5	−48.1 ± 5.5		−43.6 ± 3.8
Change from WT (mV)	−10.4	$P < 0.001$		−4.5	n.s.	

Activation voltage dependence. After data parsing, we determined activation voltage dependence by transforming *I–V* curves (Fig. 3*E*) into *G–V* curves as described in Methods. The *G–V* curve was fitted for each cell to a Boltzmann function, giving $V_{1/2}$ and slope factor (k) of the voltage-dependent response. For cells recorded manually, comparison of averages of normalized *G–V* curves for WT and S211P cells (Fig. 3*F*) revealed a hyperpolarizing shift of activation $V_{1/2}$ by the S211P mutation of 8 mV, compared to WT (Table 1). Robotic patch-clamp also

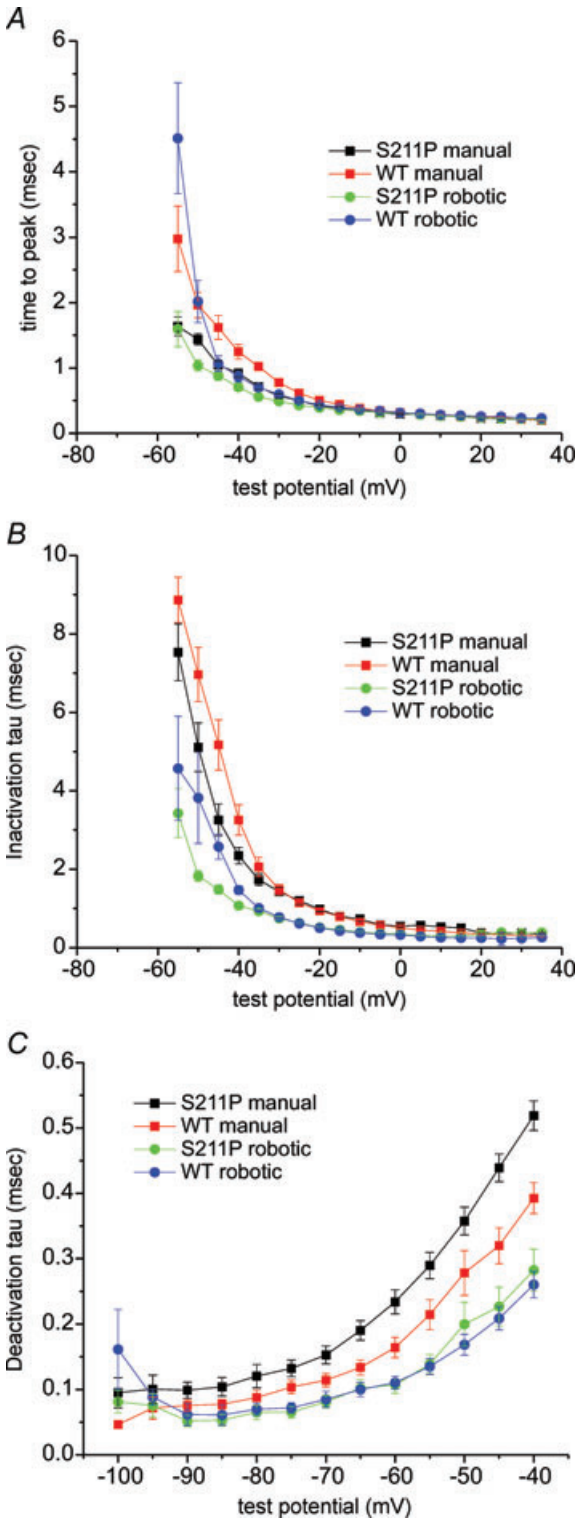

Figure 4. Channel kinetics
A, the averaged time-to-peak of the inward currents (S211P manual, black symbols ($n = 24$); S211P robotic, green symbols ($n = 14$); WT manual, red symbols ($n = 18$); WT robotic, blue symbols ($n = 28$)) measured from the activation protocol. *B*, the kinetics of current inactivation following the time-to-peak are fitted with a single exponential function. The average inactivation rate 'τ' from the fits at each pulse potential are plotted. *C*, deactivation kinetics are derived from single exponential fits to tail currents recorded in response to brief activating pulses (−20 mV for 0.4 ms) followed by a repolarization to the indicated potential. The time constants are averaged and plotted. Error bars are ± S.E.M.

revealed a hyperpolarizing shift of activation $V_{1/2}$ by the S211P, although the magnitude of the shift (11 mV) was larger (Table 1).

Time-to-peak and inactivation rate. Examination of mean time-to-peak (Fig. 4*A*) revealed a small decrease for S211P currents compared to WT currents. Manual patch-clamp showed significantly faster time-to-peak of S211P, compared to WT, channels between −55 mV and −30 mV, while robotic patch-clamp showed a faster time-to-peak for S211P over a smaller range of −55 mV and −45 mV. We also examined inactivation kinetics (Fig. 4*B*). Single exponential fits of current decay (used as a measure of time constant) showed that S211P channels tend to inactivate slightly faster over the range of −55 mV to −40 mV irrespective of whether recorded manually or robotically. Comparison of Fig. 3*A* and *B* with Fig. 3*C* and *D* indicates that activation and inactivation kinetics are faster in the robotically collected data. This may be due to the increased temperature of the robotic recording array, which averaged 4–6°C above ambient (25.4 ± 0.9°C), possibly due to the heat of 16 head-stages mounted below the planar patch-clamp array.

Deactivation. Deactivation was measured by pulsing to 0 mV to open Na^+ channels with duration just long enough to reach peak current (0.4 ms), followed by hyperpolarizing steps of 40 ms to monitor current decay as channels re-close. While manual patch-clamping revealed a small slowing of deactivation in S211P cells (Fig. 4*C*), this difference was not apparent in robotic measurements. Once again, elevated temperature of robotic recordings is predicted to contribute to the observed faster kinetics, which may have obscured slowed deactivation of the S211P mutant.

Fast inactivation. A sag in the fast inactivation data more negative than −100 mV for S211P cells studied by manual patch-clamp suggested the need for a double Boltzmann function (Fig. 5*A*). This sag is more pronounced in the robotically collected data. In both datasets, mean $V_{1/2}$ and k for the major component of fast inactivation for S211P channels were unchanged compared to WT (Table 1). Although the $V_{1/2}$ for the minor component of S211P is more hyperpolarized than WT, it did not reach statistical significance for either manual or robotic data. Slope factor for the minor component of S211P fast inactivation was shallower than WT, reaching statistical significance for

the manually collected data. The fraction of the minor component was significantly larger ($P < 0.05$) for robotic data (40%) compared to manual data (20%); this disparity may reflect the effect of higher recording temperature in the PatchXpress on recovery from slow inactivation of the channels at potential more negative than −100 mV.

Slow inactivation. Slow inactivation of $Na_v1.7$ develops over a much longer time frame (1–10 s) than fast inactivation (10–100 ms). Both manual and robotic analysis showed that slow inactivation was enhanced for S211P channels (Fig. 5*B*). Boltzmann fits for manually derived data revealed a hyperpolarizing shift of slow inactivation $V_{1/2}$ (15.1 mV) and steeper slope for S211P channels. The fraction of channels resistant to a 30 s conditioning pulse was reduced from 6.7 ± 2.2% for WT to 2.4 ± 0.6% for S211P. Boltzmann fits for robotically derived data revealed a similar hyperpolarizing shift in slow inactivation $V_{1/2}$ (14.4 mV) and steeper slope for S211P channels. The fraction of channels resistant to a 30 s conditioning pulse was reduced from 6.0 ± 2.0% for WT to 3.1 ± 1.5% for S211P.

Ramp responses. We evaluated responses of WT and S211P channels to small slow depolarizations using a ramp protocol which steadily increases from a −100 mV holding potential to +20 mV over 600 ms (0.2 mV ms^{-1}). This slow rate fully inactivates most sodium channel isoforms, but wild-type $Na_V1.7$ and many disease-causing $Na_V1.7$ mutations respond by conducting a current. To compare between cells, responses are normalized to peak inward current. Manual patch-clamping (Fig. 6*A*) clearly demonstrated an enhanced ramp response of S211P-expressing cells which averaged 1.59%, 2-fold larger than WT-expressing cells (0.78%). Robotically acquired responses to ramp protocols (Fig. 6*B*) were degraded compared to manual patch-clamp because of increased leak and noise. Although ramp responses were detectable in robotic recordings, with an average ramp response of S211P-expressing cells of 1.5%, this 1.5-fold increase over the WT response (1.0%) did not reach statistical significance.

Recovery from inactivation. Recovery from inactivation (repriming) was measured using a two-pulse protocol, varying interpulse interval and interpulse potential. Cells were first pulsed to 0 mV for 20 ms to allow complete fast inactivation and then repolarized to a specified potential for a range of durations to allow channel recovery, quantified as the ratio of the current evoked by the second pulse to 0 mV compared to the response to the first pulse. There were no significant differences in the rates of recovery between S211P and WT recorded by manual patch-clamp (Fig. 7*A* and *B*) or by robotic patch-clamp (Fig. 7*C* and *D*).

Discussion

We have compared robotic patch-clamping (Randall *et al.* 2006; Dunlop *et al.* 2008; Milligan *et al.* 2009) with manual patch-clamp analysis to assess biophysical changes produced by a previously undescribed sodium channel Nav1.7 mutation. Previously described

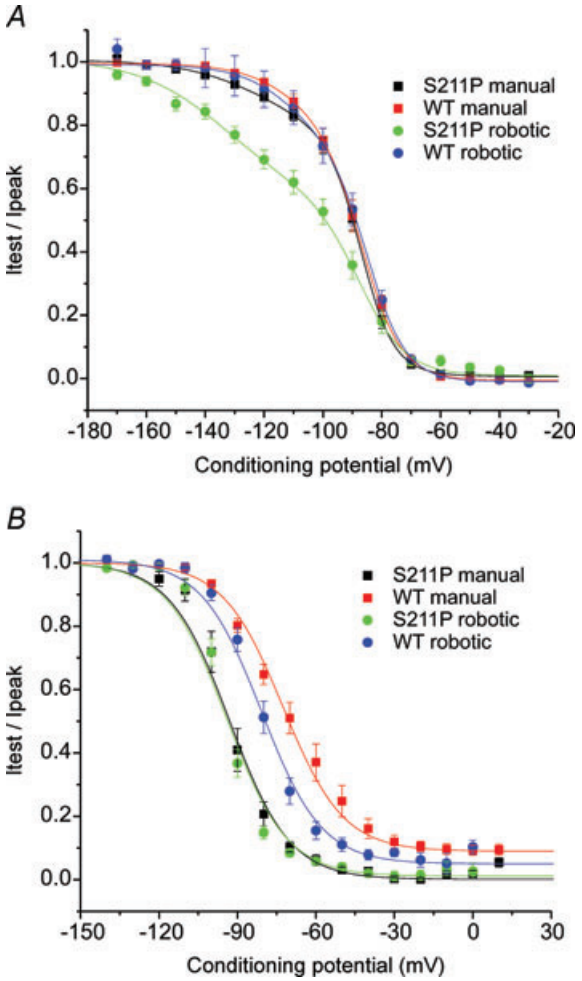

Figure 5. Inactivation properties
A, the fast inactivation protocol consists of a 500 ms conditioning pulse followed by a 40 ms test pulse to 0 mV to open the fraction of available channels. While performing Boltzmann fits of the data, it became clear that the droop at the conditioning potentials more negative than −80 mV necessitated a double Boltzmann function (S211P manual, black symbols ($n = 24$); S211P robotic, green symbols ($n = 14$); WT manual, red symbols ($n = 18$); WT robotic, blue symbols ($n = 28$)). *B*, the slow inactivation protocol consists of a 30 s conditioning pulse followed by a 100 ms pulse to −120 mV to recover from the fast inactivation state and then pulsed to 0 mV for 50 ms to activate the fraction of available channels (S211P manual, black symbols ($n = 8$); S211P robotic, green symbols ($n = 11$); WT manual, red symbols ($n = 4$); WT robotic, blue symbols ($n = 16$)). The S211P data shows a reduced availability at all potentials compared to wild-type. In addition, the S211P channels show a reduced fraction of channels that are resistant to slow inactivation at potentials more positive to −40 mV.

IEM mutations hyperpolarize activation and slow deactivation, and in many cases enhance the $Na_V1.7$ ramp current (Dib-Hajj *et al.* 2007). While all of these changes can contribute to DRG neuron hyperexcitability, the activation shift appears to be the largest contributor (Sheets *et al.* 2007). Here we show that a robotic patch-clamp and a manual patch-clamp both demonstrate that the newly identified IEM mutation S211P significantly hyperpolarizes activation. Manual patch-clamping demonstrated slowed deactivation and enhanced ramp current in S211P, while these parameters did not reach statistical significance with the robotic device that we tested, possibly because of reduced signal-to-noise ratio of the smaller currents recorded and the elevated recording temperature of the robotic platform. While the limitations that we observed may apply primarily to the specific planar patch-clamp platform that we evaluated, PatchXpress, they illustrate potential limitations that may apply more generally to robotic patch-clamp instruments, and underscore the need for validation of each measurement and protocol.

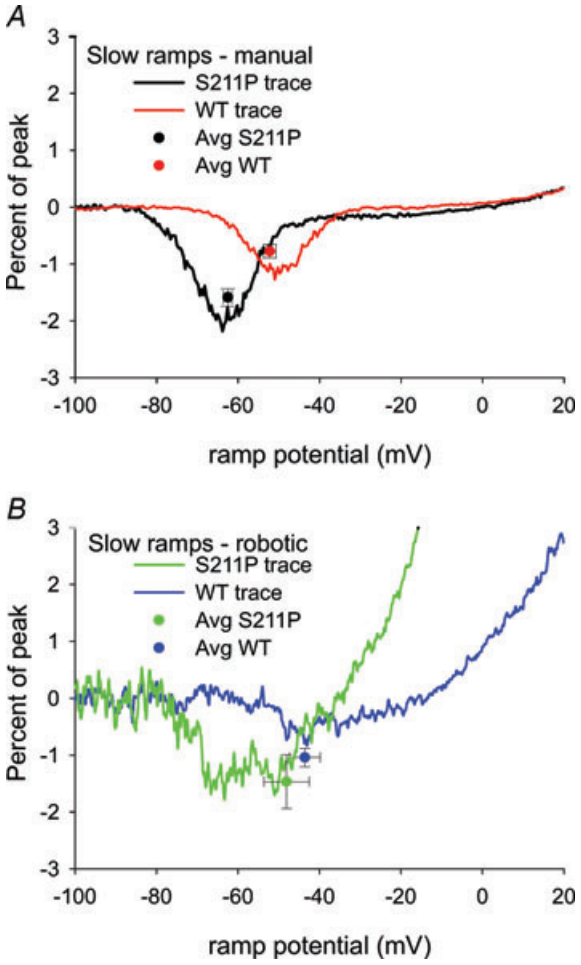

Figure 6. Slow ramp responses
A, manual patch-clamp. Typical responses to a ramp pulse protocol from −100 mV to 20 mV over 600 ms (0.2 mV ms^{-1}). The response has been rescaled as the percentage of peak inward current recorded during the activation *I–V* protocol. For display purposes the traces have been post-acquisition filtered to 500 Hz. Average peak ramp current from the S211P cells (black circle, $n = 12$) and from the WT cells (red circle, $n = 9$) are shown. *B*, robotic patch-clamp. Typical responses to a ramp pulse protocol recorded identically as by manual patch-clamp. Average peak ramp current from the S211P cells (green circle, $n = 10$) and WT cells (blue circle, $n = 20$) are shown.

Robotic and manual patch-clamping both demonstrated a large shift of slow inactivation to more hyperpolarized potentials in S211P, which may contribute to appearance of a second Boltzmann component in fast inactivation. This may be due to a fraction of channels recovering from the slow-inactivated state at the holding potential of −100 mV, which is greater for the S211P mutant, compared to WT channels. It is possible that the larger second phase recorded robotically in fast inactivation is due to a temperature-enhanced reversal of this slow inactivation during the 500 ms conditioning pulse of the fast inactivation protocol. This result is consistent with earlier studies showing that while most IEM mutations do not effect fast inactivation (Dib-Hajj *et al.* 2007), some IEM mutations enhance slow inactivation (Cummins *et al.* 2004; Choi *et al.* 2006). Enhanced slow inactivation would be expected to decrease DRG neuron excitability, but not to a degree that overcomes the shift in activation which has been shown (Sheets *et al.* 2007) to be sufficient to induce hyperexcitability.

The robotic instrument that we tested demonstrated shifts in activation voltage dependence and slow inactivation in mutant channels that were qualitatively similar to those obtained from manual patch-clamping, but did not reveal, at statistically significant levels, the slowed deactivation and enhanced ramp response demonstrated by manual patch-clamp for this mutation and most previously studied IEM mutations (Dib-Hajj *et al.* 2007). Moreover, while robotic analysis mimicked manual analysis in terms of shifts in activation and fast inactivation kinetics and in repriming, there were differences in absolute values between manual and robotic patch-clamp results, which are likely to be due to differences in ambient temperature, which might be minimized by improved temperature regulation of the robotic platform. Currently, only some robotic patch-clamp devices (Patchliner; Nanion, Germany) are manufactured with optional temperature regulation of the recording chip, and even in these devices the thermal element can only heat from ambient. Thus it is desirable that future versions of robotic patch-clamp instruments implement heating and cooling temperature regulation.

Robotic profiling, which does not screen cells prior to analysis, records simultaneously from multiple cells (16 cells for the device we used, providing throughput that is nominally 16-fold increased). Because cells

are recorded randomly without pre-selection by the robotic platform, cells with low current density, which manual patch-clampers would reject, are included in the pre-parsing robotic sample, and the lower current level and signal-to-noise level impact the population of cells that can be analysed. Thus the observed average current densities of manual and robotic datasets may not be directly comparable. Optimization of growth and cell harvesting protocols might reduce the number of cells that are recorded with poor seals and/or small currents.

When high series resistance compensation was used for robotic recording, 27% (17/64) of cells became unstable and oscillated. With the robotic device that we used, series resistance compensation for the robotic system is globally applied to all cells. Unlike manual patch-clampers who can optimize compensation for each cell by applying as much series resistance compensation as possible before onset of oscillations, the robotic device captures a larger number of cells with a lower value of series resistance compensation at which most cells are stable. We found that, with higher series resistance compensation, a criterion window for E_{Na} based on a linear fit eliminated most of the oscillating and outward current-contaminated cells, and yielded an activation $V_{1/2}$ close to the value obtained via manual cell selection. It remains to be seen whether this result is generalizable. Irrespective of this, improved seal quality via modified cell handling methods or modified recording solutions might increase the global series resistance compensation value that can be used in robotic recordings.

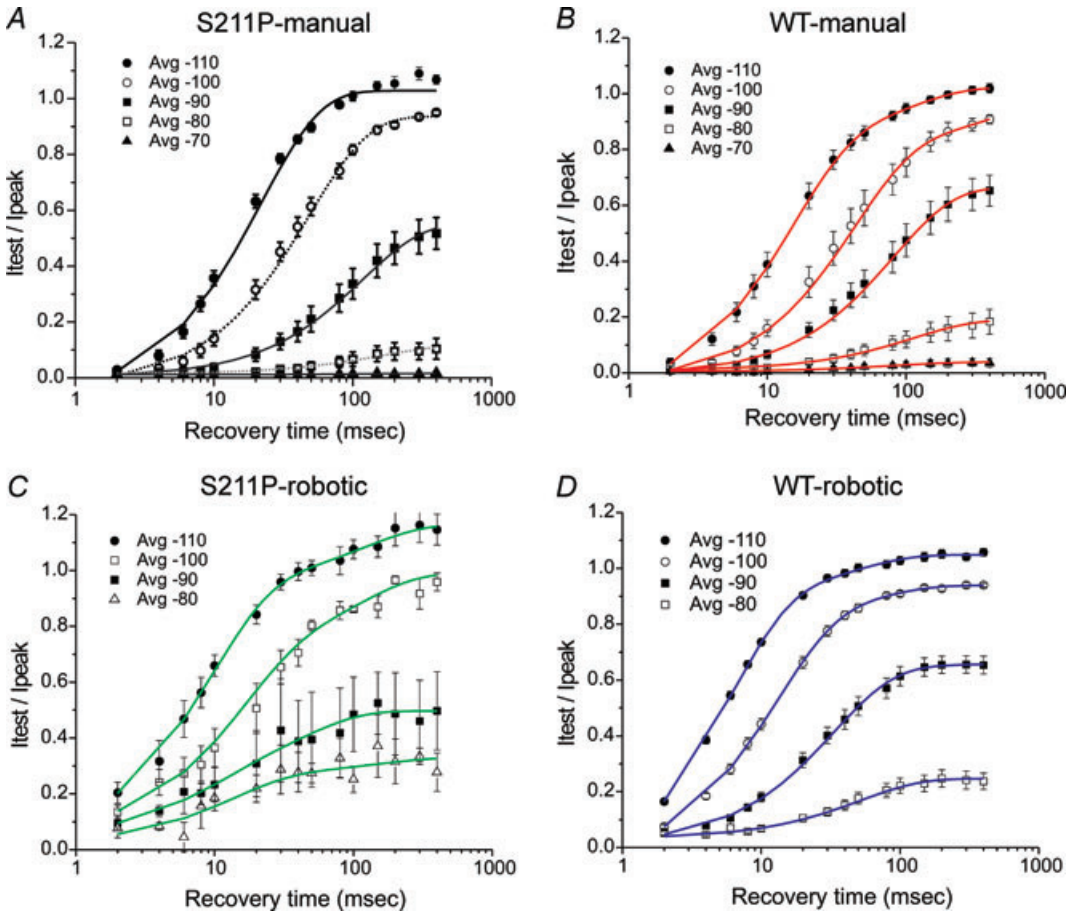

Figure 7. Recovery from inactivation

A, manual patch clamp. Fast inactivation was initiated by a step to 0 mV for 20 ms from a holding potential of −100 mV, followed by a hyperpolarizing step to a recovery potential that varied in time (2–400 ms) and amplitude (−110 to −70 mV, see legend). The recovery period was followed by a second depolarizing test pulse to 0 mV. For each recovery potential, the peak inward current in response to the test pulse was normalized by the amplitude of the response to the inactivation step and plotted as a function of recovery period duration. The averages for cells expressing S211P channels ($n = 7$) are shown with error bars ± S.E.M. *B*, the recovery from inactivation for WT channels ($n = 7$) are shown with error bars ± S.E.M. *C*, robotic patch clamp. The same pulse protocols as used for the manual dataset were programmed into the robotic platform. The averages for cells expressing S211P channels ($n = 8$) are shown with error bars ± S.E.M. *D*, the averages for cells expressing WT channels ($n = 14$) are shown with error bars ± S.E.M.

Robotic data analysis significantly reduced analysis time. For each kind of trial, e.g. activation, incremental time for the robotic system to analyse each cell was on the order of seconds. The robotic system that we tested can analyse, e.g. a dataset with 10 cells in 5 s; a larger dataset of 100 cells would add only 30 s. In contrast, manual patch-clampers often require 1–2 min per cell to perform measurements in Clampfit; including export to an external analysis program such as Origin, each cell requires 5–10 min, so that manual analysis of 10 cells can take ∼1 h and 100 cells would take ∼10 h.

Although the robotic patch-clamp that we assessed appeared to speed physiological characterization and detected some changes in channel function (activation voltage dependence, slow inactivation) that qualitatively matched manually recorded results, it failed to demonstrate statistically significant changes in other parameters (deactivation, ramp current) that we found using manual patch-clamp. While this limitation may apply in the strictest sense to the instrument we evaluated, it suggests that, in general, if robotic patch-clamping is to be used, each measurement or protocol should be validated by initial comparison to traditional, manual recording.

New planar patch-clamp platforms with chip capacities >48 cells may soon become available. Following scrutiny of results by a human physiologist and rejection of several subpopulations of cells that are typically eliminated prior to manual patch-clamp analysis, the yield of useable cells in the robotic system that we assessed was 20–60%. Extrapolating from this estimate of yields, the increase in throughput would be 3- to 10-fold for a 16-hole chip, or 9- to 30-fold for a 48-hole chip. With these cell yields, our results suggest that, with supervision and subsequent confirmation by human physiologists, robotic patch-clamp can provide screening data for selected parameters to facilitate functional assessment of mutant channels. The large number of still-uncharacterized $Na_V1.1$ (Claes *et al.* 2009; Lossin, 2009) disease-causing mutations, for example, could be assessed at a screening level by robotic profiling of transiently transfected expression constructs into HEK 293 or CHO cell lines. Robotic patch-clamp may also be useful for examining the biophysical shifts in activation and inactivation induced by systematic amino acid substitutions at specific sites (Lampert *et al.* 2008) or alanine- (McPhee *et al.* 1998) or cysteine-scanning mutagenesis (Sheets & Hanck, 2007). Refinement of cell growth and harvesting protocols, modification of recording solutions, and/or development of algorithms to select cells after gigaohm seal formation by the robotic apparatus may, in the future, improve signal-to-noise ratio and cell yield. With those modifications and improved temperature control, it is likely that robotic patch-clamp will be able to assess a larger number of channel parameters.

References

Brown AM (2009). High throughput functional screening of an ion channel library for drug safety and efficacy. *Eur Biophys J* **38**, 273–278.

Bruggemann A, George M, Klau M, Beckler M, Steindl J, Behrends JC & Fertig N (2003). High quality ion channel analysis on a chip with the NPC technology. *Assay Drug Dev Technol* **1**, 665–673.

Castle N, Printzenhoff D, Zellmer S, Antonio B, Wickenden A & Silvia C (2009). Sodium channel inhibitor drug discovery using automated high throughput electrophysiology platforms. *Comb Chem High Throughput Screen* **12**, 107–122.

Choi JS, Dib-Hajj SD & Waxman SG (2006). Inherited erythermalgia: limb pain from an S4 charge-neutral Na channelopathy. *Neurology* **67**, 1563–1567.

Claes LR, Deprez L, Suls A, Baets J, Smets K, Van Dyck T, Deconinck T, Jordanova A & De Jonghe P (2009). The SCN1A variant database: a novel research and diagnostic tool. *Hum Mutat* **30**, E904–920.

Cummins TR, Dib-Hajj SD & Waxman SG (2004). Electrophysiological properties of mutant Nav1.7 sodium channels in a painful inherited neuropathy. *J Neurosci* **24**, 8232–8236.

Dib-Hajj SD, Cummins TR, Black JA & Waxman SG (2007). From genes to pain: $Na_v1.7$ and human pain disorders. *Trends Neurosci* **30**, 555–563.

Djouhri L, Newton R, Levinson SR, Berry CM, Carruthers B & Lawson SN (2003). Sensory and electrophysiological properties of guinea-pig sensory neurones expressing Nav1.7 (PN1) Na^+ channel α subunit protein. *J Physiol* **546**, 565–576.

Dubin AE, Nasser N, Rohrbacher J, Hermans AN, Marrannes R, Grantham C, Van Rossem K, Cik M, Chaplan SR, Gallacher D, Xu J, Guia A, Byrne NG & Mathes C (2005). Identifying modulators of hERG channel activity using the PatchXpress planar patch clamp. *J Biomol Screen* **10**, 168–181.

Dunlop J, Bowlby M, Peri R, Vasilyev D & Arias R (2008). High-throughput electrophysiology: an emerging paradigm for ion-channel screening and physiology. *Nat Rev Drug Discov* **7**, 358–368.

Felts PA, Yokoyama S, Dib-Hajj S, Black JA & Waxman SG (1997). Sodium channel α-subunit mRNAs I, II, III, NaG, Na6 and hNE (PN1): different expression patterns in developing rat nervous system. *Brain Res Mol Brain Res* **45**, 71–82.

George AL Jr (2005). Inherited disorders of voltage-gated sodium channels. *J Clin Invest* **115**, 1990–1999.

Ghetti A, Guia A & Xu J (2007). Automated voltage-clamp technique. *Methods Mol Biol* **403**, 59–69.

Herzog RI, Cummins TR, Ghassemi F, Dib-Hajj SD & Waxman SG (2003). Distinct repriming and closed-state inactivation kinetics of Nav1.6 and Nav1.7 sodium channels in mouse spinal sensory neurons. *J Physiol* **551**, 741–750.

Kiss L, Bennett PB, Uebele VN, Koblan KS, Kane SA, Neagle B & Schroeder K (2003). High throughput ion-channel pharmacology: planar-array-based voltage clamp. *Assay Drug Dev Technol* **1**, 127–135.

Klugbauer N, Lacinova L, Flockerzi V & Hofmann F (1995). Structure and functional expression of a new member of the tetrodotoxin-sensitive voltage-activated sodium channel family from human neuroendocrine cells. *EMBO J* **14**, 1084–1090.

Lampert A, O'Reilly AO, Dib-Hajj SD, Tyrrell L, Wallace BA & Waxman SG (2008). A pore-blocking hydrophobic motif at the cytoplasmic aperture of the closed-state Nav1.7 channel is disrupted by the erythromelalgia-associated F1449V mutation. *J Biol Chem* **283**, 24118–24127.

Lossin C (2009). A catalog of SCN1A variants. *Brain Dev* **31**, 114–130.

McPhee JC, Ragsdale DS, Scheuer T & Catterall WA (1998). A critical role for the S4-S5 intracellular loop in domain IV of the sodium channel α-subunit in fast inactivation. *J Biol Chem* **273**, 1121–1129.

Milligan CJ, Li J, Sukumar P, Majeed Y, Dallas ML, English A, Emery P, Porter KE, Smith AM, McFadzean I, Beccano-Kelly D, Bahnasi Y, Cheong A, Naylor J, Zeng F, Liu X, Gamper N, Jiang LH, Pearson HA, Peers C, Robertson B & Beech DJ (2009). Robotic multiwell planar patch-clamp for native and primary mammalian cells. *Nat Protoc* **4**, 244–255.

Randall A, McNaughton N & Green P (2006). Properties of voltage-gated Na^+ channels in the human rhabdomyosarcoma cell-line SJ-RH30: conventional and automated patch clamp analysis. *Pharmacol Res* **54**, 118–128.

Sangameswaran L, Fish LM, Koch BD, Rabert DK, Delgado SG, Ilnicka M, Jakeman LB, Novakovic S, Wong K, Sze P, Tzoumaka E, Stewart GR, Herman RC, Chan H, Eglen RM & Hunter JC (1997). A novel tetrodotoxin-sensitive, voltage-gated sodium channel expressed in rat and human dorsal root ganglia. *J Biol Chem* **272**, 14805–14809.

Sheets MF & Hanck DA (2007). Outward stabilization of the S4 segments in domains III and IV enhances lidocaine block of sodium channels. *J Physiol* **582**, 317–334.

Sheets PL, Jackson JO 2nd, Waxman SG, Dib-Hajj SD & Cummins TR (2007). A Nav1.7 channel mutation associated with hereditary erythromelalgia contributes to neuronal hyperexcitability and displays reduced lidocaine sensitivity. *J Physiol* **581**, 1019–1031.

Tao H, Santa Ana D, Guia A, Huang M, Ligutti J, Walker G, Sithiphong K, Chan F, Guoliang T, Zozulya Z, Saya S, Phimmachack R, Sie C, Yuan J, Wu L, Xu J & Ghetti A (2004). Automated tight seal electrophysiology for assessing the potential hERG liability of pharmaceutical compounds. *Assay Drug Dev Technol* **2**, 497–506.

Toledo-Aral JJ, Moss BL, He ZJ, Koszowski AG, Whisenand T, Levinson SR, Wolf JJ, Silos-Santiago I, Halegoua S & Mandel G (1997). Identification of PN1, a predominant voltage-dependent sodium channel expressed principally in peripheral neurons. *Proc Natl Acad Sci U S A* **94**, 1527–1532.

Trivedi S, Dekermendjian K, Julien R, Huang J, Lund PE, Krupp J, Kronqvist R, Larsson O & Bostwick R (2008). Cellular HTS assays for pharmacological characterization of $Na_V1.7$ modulators. *Assay Drug Dev Technol* **6**, 167–179.

Waxman SG (2006). Neurobiology: a channel sets the gain on pain. *Nature* **444**, 831–832.

Yang Y, Wang Y, Li S, Xu Z, Li H, Ma L, Fan J, Bu D, Liu B, Fan Z, Wu G, Jin J, Ding B, Zhu X & Shen Y (2004). Mutations in SCN9A, encoding a sodium channel α subunit, in patients with primary erythermalgia. *J Med Genet* **41**, 171–174.

Author contributions

M.E. designed and performed electrophysiological experiments, analysed data and wrote the first draft of the paper. J.S.C. analysed data and edited the manuscript. E.M.E. and L.J.T. provided essential molecular biology support. Z.L., Y.L. and Y.Y. identified the patient and sequenced his and 200 matched control patient Nav1.7 genomic sequences. S.D.D.-H. and S.G.W. conceived and supervised the project and edited the manuscript. Genomic sequencing was performed in the lab of Y.Y. Electrophysiology and molecular biology was performed in the lab of S.G.W. All authors have approved the final version for publication.

Acknowledgements

We thank Bart Toftness and P. X. MacHine for excellent technical assistance. This work was supported by the Medical Research Service and Rehabilitation Research Service, Department of Veterans Affairs and by grants from the National Multiple Sclerosis Society and the Erythromelalgia Association. Additional support was provided by the Program for New Century Excellent Talents in University (NCET-06-0015 to Y.Y.) and Fok Ying Tong Education Foundation (111039 to Y.Y.). The Center for Neuroscience and Regeneration Research is a Collaboration of the Paralyzed Veterans of America and the United Spinal Association with Yale University.